FR0104314

Radiation Damage Effects in Pyrochlore and Zirconolite Ceramic Matrices for the Immobilization of Actinide-Rich Wastes

G.R. Lumpkin, B.D. Begg, and K.L. Smith

Materials Division, Australian Nuclear Science and Technology Organisation, Private Mail Bag 1, Menai, NSW 2234, Australia

ABSTRACT

Actinide-doping experiments using short-lived ^{238}Pu and ^{244}Cm have demonstrated that pyrochlore and zirconolite become fully amorphous at a dose of 0.2-0.5 x 10^{16} α/mg at ambient temperature and exhibit bulk swelling of 5-7%. Detailed studies of natural samples have included determination of the critical amorphization dose, long-term annealing rate, microstructural changes as a function of dose, and the thermal histories of the host rocks. Together, the laboratory based work and studies of natural samples indicate that the critical amorphization dose will increase by about a factor of 2-4 for samples stored at temperatures of 100-200 °C for up to 10 million years. These studies of alpha-decay damage have been complemented by heavy ion irradiation studies over the last ten years. Most of the irradiation work has concerned the critical amorphization dose as a function of temperature in thin films; however, some work has been carried out on bulk samples. The irradiation work indicates that most pyrochlore and zirconolite compositions will have similar critical amorphization doses at low temperatures (e.g., below 300-400 °C). Pyrochlores with Zr as the major B-site cation transform to a defect fluorite structure with increasing ion irradiation dose, but do not become amorphous.

INTRODUCTION

In 1998 the United States Department of Energy selected a pyrochlore-rich titanate ceramic wasteform for the disposal of surplus weapons plutonium (1). The current strategy involves storage of the ceramic wasteform as part of a "co-disposal" waste package at the Yucca Mountain site in southern Nevada. This decision represents the culmination of just over 20 years of intensive research on ceramic nuclear wasteforms, many of which contained pyrochlore, zirconolite, and other titanate phases for the incorporation of actinides and certain fission products (2-4). The development of pyrochlore and zirconolite based wasteforms for actinide-rich wastes arose from a number of the early studies that revealed their excellent chemical flexibility and durability in aqueous fluids. Both structure types are particularly well suited for the incorporation of actinides (ACTs) and rare earth elements (REEs), an important consideration for the control of nuclear criticality.

Studies of natural samples have provided a means of testing the extrapolation of laboratory data to the long time periods currently required by regulatory agencies for performance assessment. In the area of radiation damage, mineralogical studies have produced quantitative data on the crystalline-amorphous transformation and the structure of the metamict (amorphous) state (5-9). Experimental evidence has also appeared in the last ten years from heavy ion irradiation studies (8, 9). Both of these areas of research complement the existing data from actinide doping experiments carried out in the mid-1980s. Studies of samples from natural systems have also produced an enormous amount of data on the durability and alteration mechanisms in aqueous fluids. However, only limited data are currently available on the effect of radiation damage on the dissolution rates of pyrochlore and zirconolite. In this paper, we present an overview and synthesis of the actinide doping experiments, studies of natural samples, and heavy ion irradiation experiments.

CRYSTAL STRUCTURES OF PYROCHLORE AND ZIRCONOLITE

The structure of pyrochlore is considered to be an anion deficient derivative of the fluorite structure type (10-12). Numerous studies have led to the general formula $A_{2-m}B_2X_{6-w}Y_{1-n}{\cdot}pH_2O$, where A represents cations in eight fold coordination, B represents cations in six fold coordination, and X and Y are anions. The A-site accommodates cations having ionic radii of 0.086-0.155 nm, whereas the B- site incorporates cations having radii of 0.054-0.083 nm. The crystal chemistry of pyrochlore is very complicated, owing to the potential for vacancies at the A-, X-, and Y-sites (m = 0.0-1.7, w = 0.0-0.7, and n = 0.0-1.0) and the incorporation of water molecules (p = 0-2) in the

vacant tunnel sites. However, wasteform pyrochlores are designed around the ideal, stoichiometric formula $A_2B_2X_6Y$. These pyrochlores are comprised of the end-members $CaUTi_2O_7$, $CaPuTi_2O_7$, $REE_2Ti_2O_7$, and other minor components. Importantly, studies of natural samples indicate that pyrochlores can contain up to 30 wt% UO_2, 10 wt% ThO_2, 16 wt% REE_2O_3, and 10 wt% (Zr, Hf)O_2.

Zirconolite, ideally $CaZrTi_2O_7$, is also an anion deficient derivative of the fluorite structure type and can be visualized as a condensed, layered version of pyrochlore with reduced symmetry (12-15). In the structure of zirconolite-2M, the monoclinic aristotype, the Ca-site is eight coordinated and is occupied by cations having ionic radii of 0.096-0.1143 nm. The Zr-site is seven coordinated and occupied by cations with radii of 0.067-0.104 nm. Three distinct Ti-sites accommodate cations with radii of 0.0535-0.083 nm. Natural zirconolite commonly deviates from the ideal composition due to extensive coupled substitutions on the Ca- and Ti-sites, but the Zr-site is subject to only limited substitution by other elements (16). However, Vance and coworkers (17-19) have synthesized zirconolite with actinides and REEs on the Zr-site, and have confirmed many of the substitutions found in natural samples. Natural zirconolites have the ability to incorporate up to 24 wt% UO_2, 22 wt% ThO_2, and 32 wt% REE_2O_3 in the structure.

ACTINIDE DOPING EXPERIMENTS

Weber and coworkers (20, 21) examined $Gd_2Ti_2O_7$ (pyrochlore) and $CaZrTi_2O_7$ (zirconolite) doped with 3 wt% ^{244}Cm (half-life = 18 yr) and found that bulk swelling saturated at approximately 5.0-5.6% for pyrochlore and 6.0-6.5% for zirconolite. The pyrochlore and zirconolite samples became amorphous to X-rays at a dose of 0.26×10^{16} α/mg and 0.47×10^{16} α/mg, respectively. TEM results indicated that both materials exhibit isolated defect clusters (~ 2.5-5.0 nm in diameter) at dose levels of $0.05\text{-}0.10 \times 10^{16}$ α/mg. Overlap of damage clusters resulted in the appearance of a diffuse ring in electron diffraction patterns at dose levels of $0.10\text{-}15 \times 10^{16}$ α/mg. Strong mottled diffraction contrast was evident in bright field images and diffuse rings were prominent in electron diffraction patterns at doses of $0.15\text{-}0.27 \times 10^{16}$ α/mg.

The dissolution behaviour of Cm-doped $Gd_2Ti_2O_7$ and $CaZrTi_2O_7$ has been determined for the amorphous samples and for splits of the amorphous material recrystallized at 1100 °C for 12 hours (21). Samples were leached in deionized water at 90 °C for 14 days. Results of the tests indicate that the percent weight loss of both materials were higher by a factor of 2.5 in the amorphous samples. Although, none of the samples showed detectable Ti in solution, the amorphous pyrochlore showed an increase in the normalized mass loss of ^{244}Cm and its daughter product ^{240}Pu by factors of 17 and 49, respectively. In contrast, the amorphous zirconolite showed an increase in the normalized mass loss of Ca and ^{240}Pu by factors of 8 and 11, respectively. In this material, the release of ^{244}Cm was identical for the amorphous and recrystallized samples and lower than the release of ^{240}Pu in the crystalline sample by a factor of 20.

Clinard et al. (22) studied monoclinic $CaZrTi_2O_7$ doped with 5 mol% ^{238}Pu (half-life = 87 yr). After a maximum dose of 0.47×10^{16} α/mg, bulk swelling reached 5.5 vol% and neared saturation. XRD results showed that the monoclinic phase transformed to hexagonal or rhombohedral symmetry at a dose of ~ 0.11×10^{16} α/mg and became metamict at a dose of 0.3×10^{16} α/mg. Unit cell expansion determined by XRD was anisotropic, greatest along the *c* axis, and the total unit cell volume expansion reached a maximum of ~ 1 vol% at the highest measurable dose. TEM work indicated a highly crystalline structure at 0.003×10^{16} α/mg, 10-15 nm crystallites in a highly disordered matrix at ~ 0.1×10^{16} α/mg, and some residual crystallinity at ~ 0.4×10^{16} α/mg. Optical micrographs of the surface of a polished cylinder of the material showed some microcracking during the crystalline-amorphous transformation.

Clinard and coworkers (23) also investigated samples of $CaPuTi_2O_7$ held at room temperature 302 °C, and 602 °C. The bulk swelling of a sample held at ambient temperature saturated at 5.4 vol% at a dose of 0.42×10^{16} α/mg. The material became XRD amorphous at a dose of 0.28×10^{16} α/mg. For a sample held at 302 °C, bulk swelling saturated at 4.3 vol% at a dose of ~ 0.66×10^{16} α/mg. A third sample held at 602 °C remained crystalline and reached a maximum swelling of only 0.4 vol% at a dose of 0.61×10^{16} α/mg. For the sample held at ambient temperature, TEM work revealed isolated damage tracks at $0.01\text{-}0.13 \times 10^{16}$ α/mg, small crystallites in an aperiodic matrix at 0.26×10^{16} α/mg, and some residual crystallinity at $0.31\text{-}0.66 \times 10^{16}$ α/mg. Crystallinity persisted to higher doses in the sample held at 302 °C. In a similar study of Synroc doped with

^{244}Cm, Mitamura et al. (24) found that the volume expansion was reduced by a factor 2-3 for a sample held at 200°C when compared to the room temperature data.

3

NATURAL PYROCHLORE AND ZIRCONOLITE

Pyrochlore

Following the laboratory experiments described above, Lumpkin and Ewing (25) studied 51 pyrochlore samples ranging in age from 16 to 1400 Ma. Using the Th and U contents determined by electron microprobe, the dose was calculated according to the equation:

$$D = 8N_{238}(e^{\lambda 238 t} - 1) + 6N_{232}(e^{\lambda 232 t} - 1) \quad \text{(Eq. 1)}$$

In this expression, N_{238} and N_{232} are the present numbers of atoms per mg of U and Th, λ_{232} and λ_{238} are the decay constants of ^{232}Th and ^{238}U, and t is the geological age. Using XRD to determine both the beginning (D_i) of the crystalline-amorphous transformation as well as the critical amorphization dose (D_c), it was shown that the transformation zone increased in dose as a function of the geological age of the samples (Fig. 1a). Both of the dose curves shown in Figure 1a were determined by fitting the data to an equation of the form:

$$D_{i,c} = D_0 e^{tK} \quad \text{(Eq. 2)}$$

In Equation 2, D_0 is the intercept dose for D_i or D_c and K is a rate constant. These results provided independent support for the annealing of isolated alpha-recoil collision cascades back to the crystalline structure in natural pyrochlore. A more detailed analysis of the dose-age data yielded a value of $D_0 = 1.4 \times 10^{16}$ α/mg for the amorphization dose curve and $K = 1.7 \times 10^{-9}$ yr^{-1} (26).

In the natural pyrochlore samples, XRD peak intensities decrease in a regular manner with increasing dose, without transformation of the structure to the fluorite subcell, and with no major changes in peak symmetry (25). After making a correction for long-term annealing, the intensity ratios of the damaged samples were fitted to an equation of the form:

$$I/I_0 = e^{-BD} \quad \text{(Eq. 3)}$$

In this equation, B is a constant related to the amount of material damaged by each alpha-decay event. Equation 3 gave an excellent fit to the data and yielded $B = 2.6 \times 10^{-16}$ mg/α, corresponding to an average cascade diameter of 4.6 nm in which a maximum of 2600 atoms are displaced. An analysis of line broadening in these samples showed that crystallite dimensions decreased from about 500 nm to 15 nm prior to complete amorphization. The magnitude of strain increased with dose, reaching a maximum of approximately 0.003, then decreased to values below 0.0005 prior to attainment of the fully amorphous state.

Changes in the microstructure of pyrochlore have also been investigated by using high-resolution TEM (25). Mottled image contrast and local 1-5 nm sized areas of damage provided the first indication of the beginning of the crystalline-amorphous transformation. With increasing dose, local amorphous domains increased in abundance. Furthermore, some lattice misorientation (generally less than 5°) was observed in the crystalline areas at intermediate dose levels. At higher dose levels, the crystalline areas diminish in abundance, giving way to a microstructure dominated by amorphous pyrochlore. Lattice fringes were not observed at the highest dose levels, indicating that the amorphous state had been reached. Electron diffraction patterns revealed gradually diminishing Bragg spots and increasing diffuse rings with equivalent d-spacings of 0.30 and 0.18 nm. There was no definitive evidence for conversion to the fluorite subcell, e.g., the (111) diffracted beams and other superlattice spots were observed throughout the transformation. After a correction is made for long-term annealing, the transformation zone ranges from about 0.1×10^{16} α/mg to 1.2×10^{16} α/mg.

Greegor and coworkers (27-30) carried out several studies of the local structure and bonding around Ti, Nb, Ta, and U atoms in pyrochore using EXAFS-XANES. Results of these studies demonstrated that the M-O coordination polyhedra of metamict (amorphous) pyrochlore exhibit reduced bond distances, reduced coordination number, and increased distortion relative to the undamaged crystalline structure. Furthermore, there was no periodicity in evidence beyond the second coordination sphere, with some disruption of the M-M distances. From these studies it was realized that only a slight increase in the mean M-M distance was required in order to explain the overall increase in volume caused by alpha-decay damage and that this could be facilitated by increased M-O-M angles.

4

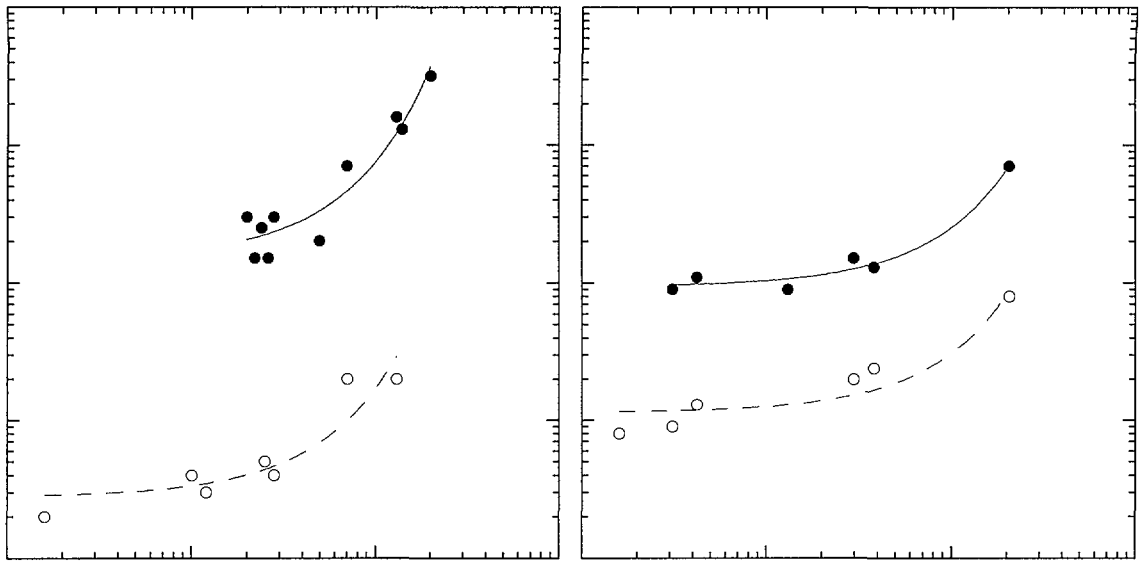

Figure 1. Dose-age data for natural pyrochlore and zirconolite. a) Data for pyrochlore were collected by XRD (25). b) Data for zirconolite collected using analytical TEM (36). The upper solid curves labelled D_c represent the critical amorphization dose and the lower dashed curves represent the onset of alpha-decay damage. The intervening regions are the crystalline-amorphous transformation zones.

Zirconolite

Electron diffraction and high-resolution TEM studies suggest that metamict zirconolite lacks periodicity beyond the second coordination sphere, consistent with a random network model of the amorphous state (31, 32). EXAFS-XANES results provide more detailed information for the Ti- and Ca-sites, demonstrating that metamict zirconolite lacks periodicity beyond the first coordination sphere, with reduced M-O bond lengths, reduced coordination number, and increased distortion of the Ti-O polyhedra (32). The reduced coordination of Ti in the metamict samples has recently been confirmed, pointing specifically to a five-fold coordination geometry (33). Additional results for the Zr-, Th-, and U-sites indicate nearly identical coordination numbers and bond lengths for the metamict and annealed samples (34). However, a reduction in medium range order (e.g., M-O-M periodicity) and a significant increase in the range of Zr-O and Th-O distances were observed, suggesting that a slight variation of the M-O-M angles can have a profound effect on long-range periodicity and medium-range order.

A detailed study of highly zoned samples from Bergell (Switzerland) and Adamello (Italy) recently provided the first detailed results on the crystalline-amorphous transformation in natural zirconolites (35). The concentrations of ThO_2 and UO_2 obtained by analytical TEM on crystals from both localities demonstrated the substantial range of alpha-decay dose in these samples. TEM work also revealed the changes in microstructure with increasing dose. Bright field, dark field, and high-resolution images illustrate the appearance of mottled diffraction contrast (0.08×10^{16} α/mg) with extensive development of amorphous domains in a crystalline matrix (0.4×10^{16} α/mg). At higher dose levels, collision cascades overlap to produce larger amorphous areas and the remaining crystalline domains are reduced in size to less than 10 nm ($0.7\text{-}0.9 \times 10^{16}$ α/mg).

Preliminary results were recently presented for seven suites of zirconolite samples ranging in age from 16 Ma to 2060 Ma and in dose from 0.008×10^{16} α/mg to 24×10^{16} α/mg (36). Using analytical TEM methods, dose "brackets" were determined and used to construct a plot of dose versus age, revealing a pattern of upward curvature with increasing age for both the onset dose and critical dose (see Fig. 1b). As in the previous work on pyrochlore, this upward curvature was interpreted as evidence for long-term annealing of isolated alpha-recoil collision cascades. The

5

data were fitted using Equation 2 in order to determine the intercept dose and annealing rate constant. Curve fits gave values of $D_0 = 0.11 \times 10^{16}$ α/mg and $K = 1.0 \times 10^{-9}$ yr^{-1} for the onset dose curve, and $D_0 = 0.94 \times 10^{16}$ α/mg and $K = 0.98 \times 10^{-9}$ yr^{-1} for the critical dose curve.

Some information is now available on the thermal histories of the natural zirconolite samples (37). In the case of the Bergell intrusion, the thermal history is well constrained by thermochronology, a method of time-temperature path analysis that relies on age dating techniques with different closure temperatures (e.g., U-Th-Pb, K-Ar, Rb-Sr, and fission track dating). From these data, an average effective temperature of 185 °C was calculated for the intrusion. Using a simple model of conductive heat flow together with the available geological information, estimates of the average effective temperature were derived for four other zirconolite localities. The combined data indicate that the zirconolites have been stored in the Earth's crust at average temperatures of 100-200°C (certain pyrochlores studied earlier, e.g., references 25 and 26, are from some of the same localities and therefore experienced the same P-T-t history).

HEAVY ION IRRADIATION

In one of the first studies of pyrochlore or zirconolite, Ewing and Wang (38) irradiated a thin TEM sample of recrystallized natural zirconolite using 1.5 MeV Kr ions and showed that the zirconolite became amorphous after a dose of 4×10^{14} ions/cm^2. Subsequent work on synthetic zirconolite samples and U-doped pyrochlore revealed that D_c ranges from 3.5×10^{14} ions/cm^2 to 6.1×10^{14} ions/cm^2 at room temperature, with no systematic variation as a function of composition or polytype (39).

Wang et al. (40) recently examined the temperature dependence of amorphization of $Gd_2Ti_2O_7$ and $CaZrTi_2O_7$ thin films. Results for 1.0 MeV Kr ions revealed critical temperature (T_c) values of 837 °C for the pyrochlore and 381 °C for the zirconolite. T_c is the critical temperature above which amorphization cannot occur (the annealing rate is greater than the damage production rate). Recent studies of the temperature dependence of D_c have been carried out for a number of zirconolite compositions (41, 42) and analyzed using the simple model given below:

$$D_c = \frac{D_o}{1 - \exp\left[\frac{E_a}{k}\left(\frac{1}{T_c} - \frac{1}{T}\right)\right]} \qquad \text{(Eq. 4)}$$

In Equation 4, D_0 is the critical dose at zero Kelvin, E_a is the activation energy for irradiation-enhanced annealing of damage, and k is Boltzmann's constant. The data of Wang et al. (41) indicate T_c values of 277-747 °C and activation energies of 0.2-0.4 eV for five different zirconolite compositions (see Fig. 2a). In this work, the range of T_c values correlates with composition, generally increasing with the level of Ce and Nd substitution. Similar results have been presented by Smith et al. (42) for two $CaZrTi_2O_7$ samples prepared at 1200 °C and 1450 °C and having different levels of crystallographic perfection (Fig. 2b). Smith et al. (42) also demonstrated that these data are non-linear in plots of $\ln(1-D_0/D_c)$ versus 1/T, indicating that the simple model of Equation 4 relating the activation energy, critical temperature, and critical dose does not adequately explain the results.

In $A_2Ti_2O_7$ pyrochlores with A = Y, Sm, Gd and Lu, heavy ion irradiation work has shown no significant effect of A-site ion mass or size on the temperature dependence of the critical dose for amorphization (43). In each case the dose for amorphization at room temperature was found to be approximately 0.5×10^{14} ions/cm^2. In stark contrast, pyrochlores of $Gd_2(Ti_{2-x}Zr_x)O_7$ stoichiometry display a dramatic decrease in susceptibility to radiation induced amorphization as a function of increasing Zr content, with the end member $Gd_2Zr_2O_7$ being totally resistant to amorphization (44, 45). Dissolution experiments using a pH 2 solution at 90 °C have been performed on some of these samples, but the results are not totally consistent. The leach rates of Gd and Ti increased by a factor of ~10 in the amorphous sample of $Gd_2Ti_2O_7$ relative to the crystalline sample. For $Lu_2Ti_2O_7$, the leach rates of Lu and Ti increased by factors of about 5 and 9, respectively, due to amorphization. Interestingly, no significant effect of radiation damage was observed for the leach rate of Y in $Y_2Ti_2O_7$. In this sample, the initial Ti leach rate was increased by a factor of 6 in the amorphous sample, but this decreased over the duration of the test (43).

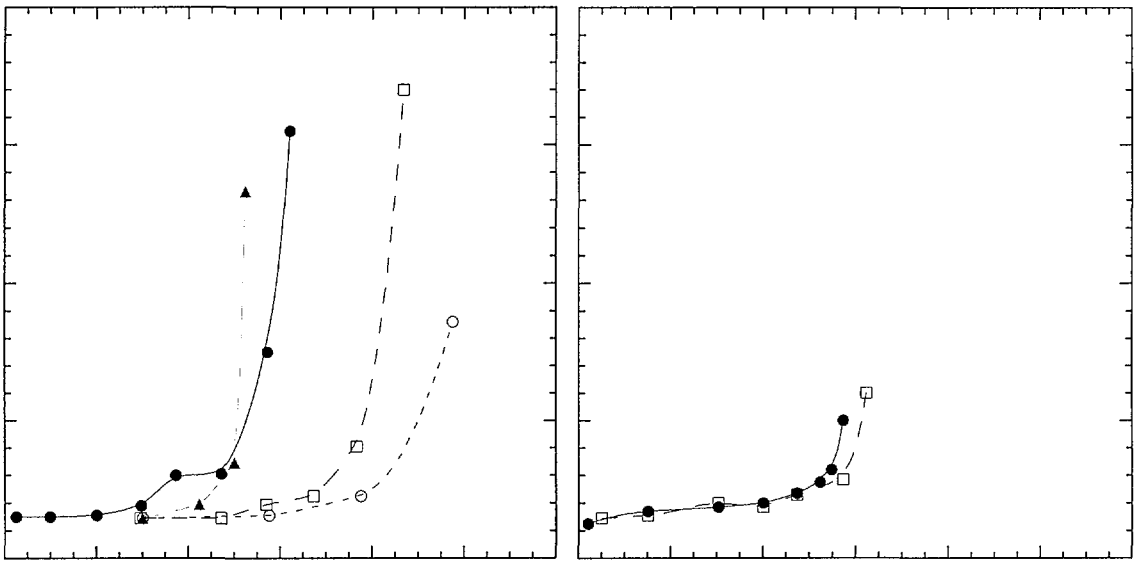

Figure 2. Heavy ion irradiation data for thin TEM specimens of zirconolite. a) Selected data from Wang et al. (41). Note the large range in the T_c that varies with composition. b) Data from Smith et al. (42) for end-member zirconolite prepared at 1200 °C (2M polytype with stacking disorder) and 1450 °C (perfect 2M). Stacking disorder has little effect on the temperature dependence. All data sets have a similar critical amorphization dose at temperatures below about 473 K (200 °C).

Certain pyrochlores undergo an irradiation-induced transformation to a defect fluorite structure, although the stability of the resulting structure is highly dependent on the ionic radii ratio of the original pyrochlore (46). Pyrochlores with an ionic radius ratio of $r_A/r_B \leq 1.52$ (for instance $Gd_2(Ti_{2-x}Zr_x)O_7$ with $x \geq 1.5$) transform to a stable radiation resistant fluorite-structure after irradiation with 2 MeV Au^{2+} to a dose of 5×10^{14} ions/cm^2. However as the ionic radius ratio of the pyrochlore increases beyond $r_A/r_B > 1.52$, e.g., $Gd_2(Ti_{2-x}Zr_x)O_7$ with $x < 1.5$, fluorite becomes increasingly unstable with respect to the amorphous state. No fluorite was observed in the similarly irradiated $Gd_2(Ti_{2-x}Zr_x)O_7$ with $x = 0.5$ or $Gd_2Ti_2O_7$ samples ($r_A/r_B \geq 1.66$). Similar results have been reported for the pyrochlores $NaCaNb_2O_6F$ and $NaCaTa_2O_6F$, both of which have $r_A/r_B = 1.80$ (47).

DISCUSSION

Studies of actinide doped and natural samples indicate that pyrochlores with Ti, Nb, and Ta as the major B-site cations become amorphous as a result of the gradual accumulation of alpha-recoil collision cascades until the material becomes aperiodic. Heavy ion irradiation studies generally confirm these results and show that the temperature dependence of the critical amorphization dose may vary dramatically. For the pyrochlore structure type, this may be a direct result of the composition as expressed by the radius ratio r_A/r_B. In particular, pyrochlores with $r_A/r_B \leq 1.52$ transform to a defect fluorite structure that is resistant to amorphization by heavy ion irradiation.

The dose curves for natural pyrochlore and zirconolite indicate critical dose values of approximately 1.4×10^{16} α/mg and 0.9×10^{16} α/mg, respectively. A comparison with laboratory studies of pyrochlore and zirconolite doped with ^{238}Pu and ^{244}Cm shows that the critical dose

7

values of natural pyrochlore and zirconolite are higher by a factor of approximately 2-4. This result is probably due to the higher temperatures (100-200°C) experienced by the natural samples in their host rocks, a proposal that is consistent with the laboratory data for samples of $CaPuTi_2O_7$ and Cm-doped zirconolite stored at elevated temperatures (23, 24). The dose-age data also provide evidence for the long-term annealing of isolated alpha-recoil collision cascades in pyrochlore and zirconolite. These results indicate that further increases in the critical amorphization dose due to long-term annealing will not occur for time periods of less than approximately 10 million years. The available data from dissolution tests of amorphous and crystalline samples indicate some increase in leach rates due to amorphization, but the data are not entirely consistent and require confirmation.

REFERENCES

1 B.R. Myers, G.A. Armantrout, C.M. Jantzen, A. Jostsons, J.M. McKibben, H.F. Shaw, D.M. Strachan, and J.D. Vienna, Technical Evaluation Panel Summary Report, Plutonium Immobilization Project, Report No. UCRL-ID-129315, 1998.

2 A.E. Ringwood, S.E. Kesson, K.D. Reeve, D.M. Levins, and E.J. Ramm, in: W. Lutze and R.C. Ewing (Eds.), Radioactive Waste Forms for the Future, North-Holland, Amsterdam, 1988, p. 233.

3 A.B. Harker, in: W. Lutze and R.C. Ewing (Eds.), Radioactive Waste Forms for the Future, North-Holland, Amsterdam, 1988, p. 335.

4 C.J. Ball, W.J. Buykx, F.J. Dickson, K. Hawkins, D.M. Levins, R.St.C. Smart, K.L. Smith, G.T. Stevens, K.G. Watson, D. Weedon, and T.J. White, J. Am. Ceram. Soc. 72 (1989) 404.

5 R.C. Ewing, B.C. Chakoumakos, G.R. Lumpkin, and T. Murakami, Mater. Res. Soc. Bull. 12 (1987) 58.

6 R.C. Ewing, B.C. Chakoumakos, G.R. Lumpkin, T. Murakami, R.B. Greegor, and F.W. Lytle, Nucl. Instr. Meth. Phys. Res. B32 (1988) 487.

7 R.C. Ewing, Nucl. Instr. Meth. Phys. Res. B91 (1994) 22.

8 R.C. Ewing, W.J. Weber, and F.W. Clinard Jr., Prog. Nucl. Energy 29 (1995) 63.

9 W.J. Weber, R.C. Ewing, C.R.A. Catlow, T. Diaz de la Rubia, L.W. Hobbs, C. Kinoshita, Hj. Matzke, A.T. Motta, M. Nastasi, E.K.H. Salje, E.R. Vance, and S.J. Zinkle, J. Mater. Res. 13 (1998) 1434.

10 M.A. Subramanian, G. Aravamudan, and G.V. Subba Rao, Prog. Solid State Chem. 15 (1983) 55.

11 B.C. Chakoumakos, J. Solid State Chem. 53 (1984) 120.

12 K.L. Smith and G.R. Lumpkin, in: J.N. Boland, J.D. Fitz Gerald (Eds.), Defects and Processes in the Solid State: Geoscience Applications, the McLaren Volume, Elsevier, Amsterdam, 1993, p. 401.

13 B.M. Gatehouse, I.E. Grey, R.J. Hill, and H.J. Rossell, Acta Crystallogr. B37 (1981) 306.

14 W. Sinclair and R.A. Eggleton, Am. Mineral. 67 (1982) 615.

15 H.J. Rossell, J. Sol. State Chem. 99 (1992) 38.

16 R. Gieré, C.T. Williams, and G.R. Lumpkin, Schweiz. Mineral. Petrogr. Mitt. 78 (1998) 433.

17 E.R. Vance, B.D. Begg, R.A. Day, and C.J. Ball, in: T. Murakami and R.C. Ewing (Eds.), Scientific Basis for Nuclear Waste Management XVIII, Mater. Res. Soc. Symp. Proc. 353 (1995) 767.

18 B.D. Begg, E.R. Vance, R.A. Day, M. Hambley, and S.D. Conradson, in: W.J. Gray and I.R. Triay (Eds.), Scientific Basis for Nuclear Waste Management XIX, Mater. Res. Soc. Symp. Proc. 465 (1997) 325.

19 B.D. Begg and E.R. Vance, in: W.J. Gray and I.R. Triay (Eds.), Scientific Basis for Nuclear Waste Management XIX, Mater. Res. Soc. Symp. Proc. 465 (1997) 333.

20 W.J. Weber, J.W. Wald, and Hj, Matzke, Mater. Lett. 138 (1985) 173.

21 W.J. Weber, J.W. Wald, and Hj, Matzke, J. Nucl. Mater. 138 (1986) 196.

22 F.W. Clinard Jr., D.L. Rohr, and R.B. Roof, Nucl. Instr. Meth. Phys. Res. B1 (1984) 581.

23 F.W. Clinard Jr., D.E. Peterson, D.L. Rohr, and L.W. Hobbs, J. Nucl. Mater. 126 (1984) 245.

24 H. Mitamura, S. Matsumoto, T. Miyazaki, T.J. White, K. Nukaga, Y. Togashi, T. Sagawa, S. Tashiro, D.M. Levins, and A. Kikuchi, J. Am. Ceram. Soc. 73 (1990) 3433.

25 G.R. Lumpkin and R.C. Ewing, Phys. Chem. Minerals 16 (1988) 2.

26 G.R. Lumpkin, K.P. Hart, P.J. McGlinn, T.E. Payne, R. Gieré, and C.T. Williams, Radiochim. Acta 66/67 (1994) 469.

27 R.B. Greegor, F.W. Lytle, B.C. Chakoumakos, G.R., Lumpkin, and R.C. Ewing, in: C.M. Jantzen, J.A. Stone, and R.C. Ewing (Eds.), Scientific Basis for Nuclear Waste Management VIII, Mater. Res. Soc. Symp. Proc. 44 (1985) 655.

28 R.B. Greegor, F.W. Lytle, B.C. Chakoumakos, G.R., Lumpkin, and R.C. Ewing, in: L.O. Werme (Ed.), Scientific Basis for Nuclear Waste Management IX, Mater. Res. Soc. Symp. Proc. 50 (1985) 387.

29 R.B. Greegor, F.W. Lytle, B.C. Chakoumakos, G.R., Lumpkin, R.C. Ewing, C.L. Spiro, and J. Wong, in: J.K. Bates and W.B. Seefeldt (Eds.), Scientific Basis for Nuclear Waste Management X, Mater. Res. Soc. Symp. Proc. 84 (1987) 645.

30 R.B. Greegor, F.W. Lytle, B.C. Chakoumakos, G.R., Lumpkin, J.K. Warner, R.C. Ewing, in: W. Lutze and R.C. Ewing (Eds.), Scientific Basis for Nuclear Waste Management XII, Mater. Res. Soc. Symp. Proc. 127 (1989) 261.

31 R.C. Ewing and T.J. Headley, J. Nucl. Mater. 119 (1983) 102.

32 G.R. Lumpkin, R.C. Ewing, B.C. Chakoumakos, R.B. Greegor, F.W. Lytle, E.M. Foltyn, F.W. Clinard Jr., L.A. Boatner, and M.M. Abraham, J. Mater. Res. 1 (1986) 564.

33 F. Farges, Am. Mineral. 82 (1997) 44.

34 F. Farges, R.C. Ewing, and G.E. Brown Jr., J. Mater. Res. 8 (1993) 1983.

35 G.R. Lumpkin, K.L. Smith, and R. Gieré, Micron 28 (1997) 57.

36 G.R. Lumpkin, K.L. Smith, M.G. Blackford, R. Gieré, and C.T. Williams, in: I.G. McKinley and C. McCombie (Eds.), Scientific Basis for Nuclear Waste Management XXI, Mater. Res. Soc. Symp. Proc. 506 (1998) 215.

37 G.R. Lumpkin, R.A. Day, P.J. McGlinn, T.E. Payne, R. Gieré, and C.T. Williams, in: D.J. Wronkiewicz and J.H. Lee (Eds.), Scientific Basis for Nuclear Waste Management XXII, Mater. Res. Soc. Symp. Proc. 556 (1999) 793.

38 R.C. Ewing and L.M. Wang, Nucl. Instr. Meth. Phys. Res. B65 (1992) 319.

39 K.L. Smith, N.J. Zaluzec, and G.R. Lumpkin, J. Nucl. Mater. 250 (1997) 36.

40 S.X. Wang, L.M. Wang, R.C. Ewing, G.S. Was, and G.R. Lumpkin, Nucl. Instr. Meth. Phys. Res. B148 (1999) 704.

41 S.X. Wang, G.R. Lumpkin, L.M. Wang, and R.C. Ewing, Nucl. Instr. Meth. Phys. Res. B166-167 (2000) 293-298.

42 K.L. Smith, M.G. Blackford, G.R. Lumpkin, and N.J. Zaluzec, Scientific Basis for Nuclear Waste Management XXIII (2000) in press.

43 B.D. Begg, W.J. Weber, R. Devanathan, J.P. Icenhower, S. Thevuthasan, and B.P. McGrail, Ceram. Trans. 107 (2000) 553.

44 S.X. Wang, B.D. Begg, L.M. Wang, R.C. Ewing, W.J. Weber, and K.V.G. Kutty, J. Mater. Res. 14 (1999) 4470.

45 S.X. Wang, L.M. Wang, R.C. Ewing, and K.V. Govidan Kutty, in: S.J. Zinkle, G.E. Lucas, R.C. Ewing, and J.S. Williams, Microstructural Processes in Irradiated Materials, Mater. Res. Soc. Symp. Proc. 540 (1999) 355.

46 B.D. Begg, N.J. Hess, D.E. McCready, S. Thevuthasan, and W.J. Weber, J. Nucl. Mater., in press.

47 G.R. Lumpkin, K.L. Smith, and M.G. Blackford, J. Nucl. Mater. in press.